Available online at www.sciencedirect.com
ScienceDirect
Trans. Nonferrous Met. Soc. China 28(2018) 1745−1754
Transactions of Nonferrous Metals Society of China
www.tnmsc.cn

In vitro degradation and cytotoxicity of Mg−5Zn−0.3Ca/nHA biocomposites prepared by powder metallurgy

Neda ABOUDZADEH[1], Changiz DEHGHANIAN[1], Mohammad Ali SHOKRGOZAR[2]

1. School of Metallurgy and Materials Engineering, College of Engineering, University of Tehran, P. O. Box 14155-6455, Tehran, Iran;
2. National Cell Bank, Pasteur Institute of Iran, P. O. Box 1316943551, Tehran, Iran

Received 6 August 2017; accepted 16 May 2018

Abstract: Mg−5Zn−0.3Ca/nHA biocomposites were prepared from pure Mg, Zn, Ca and nano-hydroxyapatite (nHA) powders by powder metallurgy method. The effect of various mass fractions of nHA (1%, 2.5%, 5%) as reinforcement on the corrosion properties of Mg−5Zn−0.3Ca alloy was investigated. The corrosion resistance of biocomposite samples was investigated by immersion tests and electrochemical techniques in SBF solution. The results showed that the corrosion resistance of Mg alloy was improved by adding 1% and 2.5% nHA. Bioactive nHA motivated the formation of stable phosphate and carbonate layers on surface and improved corrosion resistance of nanocomposites. However, addition of large contents of nHA in Mg alloy as reinforcement increased the density of this precipitated layer, so gases produced from localized corrosion were accumulated underneath this layer and decreased its adhesiveness and lowered its corrosion resistance. Indirect cytotoxicity evaluation for Mg alloy and its nanocomposites also showed that their extraction was not toxic and nanocomposite with 1% nHA indicated almost similar behavior as negative control.

Key words: powder metallurgy; metal biocomposite; corrosion; magnesium

1 Introduction

Magnesium (Mg) is a metallic biomaterial with bioresorbable property [1] which has been chosen as a candidate for bone tissue engineering [2]. Good biocompatibilities and mechanical properties of Mg alloys as temporary biomaterials are the main advantages for that [2]. High degradation rate of Mg is the main concern for its implementation as an orthopedic biomaterial [3]. Destruction of Mg implant due to corrosion occurs prior to a formation of stable tissue around it. Therefore, prevention of Mg corrosion is significant [4,5]. Several approaches such as alloying [2,4,6−8], compositing [9−12] and coating [13,14] were investigated for optimizing corrosion resistance and mechanical properties of Mg to make it suitable for bone tissue repairing. In the present work, both alloying and compositing processes were used to fabricate Mg−5Zn−0.3Ca/*n*HA nanocomposites and to consider the effect of different contents of nHA on corrosion properties of Mg−5Zn−0.3Ca alloy.

Bioactivity, mechanical and corrosion properties of Mg alloys have been improved by compositing with bioactive materials such as HA [15]. A few works have been published to indicate modification in corrosion resistance of Mg alloys by compositing with nano size HA (nHA). FENG and HAN [10] prepared magnesium alloy matrix composite of ZK60A reinforced with ultrafine calcium phosphate and reported that metal matrix composite (MMC) had lower corrosion rate than Mg alloy. In vitro, the results indicated that nano sized HA could significantly improve the bioactivity and osteoconductivity [9]. AHMADKHANIHA et al [11] reported that addition of nHA particles into Mg by friction stir process (FSP) caused the corrosion resistance of pure Mg to increase. RAZAVI et al [9] fabricated nano composite of AZ91/20% (mass fraction) nano fluorapatite (FA) and showed that mechanical properties and corrosion resistance of the composites were enhanced by adding FA.

Most of recent studies focus on compositing Mg or industrial alloy of Mg (like AZ31, AZ91 and WE43) with HA. In this work, a biocompatible alloy of Mg

Corresponding author: Changiz DEHGHANIAN; Tel/Fax: +98-2161114103; E-mail: cdehghan@ut.ac.ir
DOI: 10.1016/S1003-6326(18)64818-6

(Mg−5Zn−0.3Ca) was selected as matrix and nano sized HA was selected as reinforcement. According to literature, alloying elements like Al and some rare earth elements in industrial alloys of Mg enhanced corrosion resistance but would cause latent toxicity with harmful effect on the human body during degradation [2,16]. Studies have indicated that elements such as Zn [4], Mn [17], Zr [18] and Ca [2] could improve both mechanical properties and corrosion resistance of Mg without any health problems. In fact, most of these elements are essential for body metabolism [6]. In this work, a biocompatible Mg alloy with nano sized HA as reinforcement was selected and the corrosion resistance of Mg−5Zn−0.3Ca/nHA nanocomposite prepared by powder metallurgy was investigated. In addition, the effect of different contents of nHA on properties of the composites was also examined.

2 Experimental

2.1 Material preparation

Nanocomposites of Mg−5Zn−0.3Ca/nHA with different contents of nHA were synthesized by powder metallurgy method. Initially, the pure powders of Mg (S5430817 002, Merck), Zn (K39617189 929, Merck) and Ca (S5101853 907, Merck) were blended, and then nHA powder was added into the mixture in different contents of 0, 1%, 2.5% and 5% (mass fraction). The nHA powders were synthesized in the size of 70−100 nm by precipitation method [19]. Prepared samples were classified as MZC, MZC-1nHA, MZC-2.5nHA and MZC-5nHA, respectively. Each mixture of powder was separately fast-milled for 6 min and then pressed by a uniaxial press at 400 MPa into the size of *d*10 mm × 5 mm and heated at a rate of 10 °C/min to reach 550 °C in a tube furnace in the argon atmosphere for 2 h.

2.2 Microstructure characterization

Optical microscopy (OM) was used to characterize the microstructure of nanocomposites. The standard metallographic procedure was applied for the sample preparation. The surface of specimens was first ground with abrasive SiC paper from 600 to 2500 grades, and then polished with diamond paste (3 and 1 μm) and etched with fresh nital solution (2%).

X-ray diffraction (XRD, JDX−8030, Jeol, Japan) with Cu K_α source was used to obtain the diffraction patterns for nanocomposites. The identification of all reflections was accomplished using the X'Pert software. Scanning electron microscopy (SEM, TSCAN-VEGA, China) and energy dispersive X-ray spectroscopy (EDS, TSCAN-VEGA, China) were used to identify micro structure and elemental analyses of nanocomposite samples. Morphology and functional groups in the corrosion product were also characterized by SEM and Fourier transform infrared spectroscopy (FTIR, 8400S, SHIMADZU, Japan), respectively.

2.3 Corrosion measurements

Corrosion properties of nanocomposites were evaluated by immersion and electrochemical methods. The corrosion tests were carried out in the simulated body fluid (SBF) which was prepared according to Kokubo's protocol [20]. The surface of prepared specimens were ground with 600−2000 grade SiC abrasive paper and then sonicated in the acetone bath for 3 min before starting the corrosion measurement.

2.3.1 Electrochemical corrosion tests

The electrochemical corrosion tests were done by conventional three-electrode cell using the sample as working electrode, saturated calomel electrode (SCE) as reference and platinum mesh as counter. Anodic potentiodynamic polarization tests were done employing a Metrohm Autolab PGSTAT 30. The potential was polarized from −0.2 to +0.5 V with respect to open-circuit potential (OCP) at a scan rate of 1 mV/s. Corrosion resistance of nanocomposites was determined from polarization curves by Tafel extrapolation.

Electrochemical impedance spectroscopy (EIS) tests were also carried out using an AC impedance analyzer (Solortron, 1260) after reaching a stable OCP. The frequency range was varied from 0.1 Hz to 100 kHz. Commercial ZSimpwin software (version 3.4) was used to analyze the acquired experimental data and the best-fitted equivalent circuit model was found. Each test was repeated twice to evaluate the accuracy of the test results.

2.3.2 Immersion tests

The mass loss tests for the specimens were carried out according to ASTM G31−72 [21]. The cleaned specimens in the size of 10 mm in diameter and 5 mm in thickness were weighted with 0.0001 g in accuracy and then each one was immersed in 15 mL SBF for different time periods of 6, 24, 48, 72, 168 and 336 h under the physiological condition of 5% CO_2 at 37 °C. After each immersion time, samples were rinsed with distilled water and dried at room temperature. The surface corrosion product of samples was cleaned using chromic acid [22] before mass measurement. The corrosion rate (C_R) of nanocomposites was calculated as follows:

$$C_R = \frac{KW}{DAt} \quad (1)$$

where K is a constant value of 3.45×10^6, W is mass loss in g, D is density in g/cm^3, A is the initial surface area in cm^2 and t is immersion time in h. The morphology of

precipitated layers on the surface of samples after immersing in SBF for 72 h was also investigated by SEM. After each immersion time, the concentration of Mg ions in SBF was also measured by atomic absorption spectroscopy (AAS, SHIMADZU, Japan). In addition, the volume of emitted hydrogen related to magnesium dissolution was assessed for nanocomposites in SBF. The setup of a typical H_2^{evo} experiment was used [23,24]. First, nanocomposites were submerged in SBF and then an inverted funnel and burette which was filled with SBF was placed directly above them to capture H_2 gas.

2.4 MTT assay

Indirect contact method in compliance with ISO 10993−12 [25] was selected to investigate the toxicity of nanocomposites by MTT (3-(4,5-dimethylthiazol-2-yl)–2,5–diphenyltetrazolium bromide) assay. The nanocomposite specimens were sterilized by autoclave and each specimen was separately incubated in Roswell Park Memorial Institute medium (RPMI/1640) containing 10% fetal bovine serum (FBS; Gibco) with the ratio of 3 mL/cm^2 area of samples in order to get the extraction media. The extraction media were collected at 3, 5 and 7 days after incubation. The MG63 cells were seeded in each well of a 48-well plate for 24 h, and then the cell media were replaced with the sample extract media and incubated at 37 °C with 5% CO_2. The MG63 cultured wells with no replacing media were used as negative controls. After 24 h, the medium of each well was removed and 10 μL of MTT (Sigma, USA) was added to each well and incubated again for 5 h. After that, the MTT solution was removed and 100 μL/well of isopropanol (Sigma, Milwaukee, USA) was added to dissolve the formazan crystals and again incubated for 10 min. Finally, the plate was placed in a cold room for 15 min prior to absorbance measurements. A multi-well microplate reader (ICN, Switzerland) at 570 nm was used to record the optical density (OD, O) of wells. The cell relative growth rate (RGR, G) was calculated by

$$G=(O_{sample}/O_{control})\times 100\% \quad (2)$$

The accuracy of results was ascertained by repetition of each test for five times. The significant differences of RGR in MTT assay were analyzed by the analysis of variance (ANOVA) technique in SPSS software (Ver 20.0) when the statistical significance value (p) was defined as 0.05.

3 Results and discussion

3.1 Microstructure

The XRD patterns for MZC, MZC-1nHA, MZC-2.5nHA and MZC-5nHA samples are shown in Fig. 1. Characteristic diffraction of HA was revealed in XRD pattern for nanocomposites in Figs. 1(b−d). The X-ray diffraction patterns of MZC and other nanocomposites showed peaks of intermetallic phases of $MgZn_2$, $MgZn_{5.31}$, Mg_2Ca and $Ca_2Mg_6Zn_3$, and thus eutectic transformations happened in sintering process. These intermetallic phases could improve corrosion resistance of Mg [2,4]. ZHANG et al [7] fabricated the Mg−Zn alloy in different contents of Zn by casting method, and MgZn phase patterns were detected for the alloys with Zn mass fraction more than 5%. The presence of $Ca_2Mg_6Zn_3$ phase was also detected in Mg−5.12%Zn−0.32%Ca (mass fraction) alloy prepared by casting method [26]. Figure 1 also revealed that there was no significant difference between X-ray diffraction patterns for nanocomposites with different content of nHA. It seemed that there was no obvious reaction between the nHA and metal matrix in the sintering process.

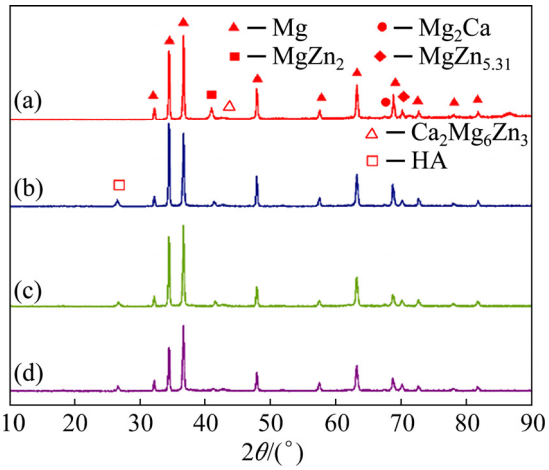

Fig. 1 XRD patterns of MZC (a), MZC-1nHA (b), MZC-2.5nHA (c) and MZC-5nHA (d)

Metallographic microstructures of nanocomposites after sintering process are shown in Fig. 2. The results indicated that the grain size for the nanocomposites was reduced by increasing nHA content. The nano sized particles might attach to the metal particle through mixing in fast mill and pined grain boundaries and prevented from grain growth in sintering process [27]. Therefore, the nano composites with higher contents of nHA had smaller grain sizes.

The SEM micrographs of MZC and nanocomposites are illustrated in Fig. 3. It can be seen that the lamellar second phases formed along the grain boundaries and their triple junction. The EDS results of marked points in Fig. 3 are listed in Table 1. The EDS results showed that there were Mg, Zn, Ca and P elements in second phases in grain boundaries in nanocomposites and only Mg and Zn presented in matrix.

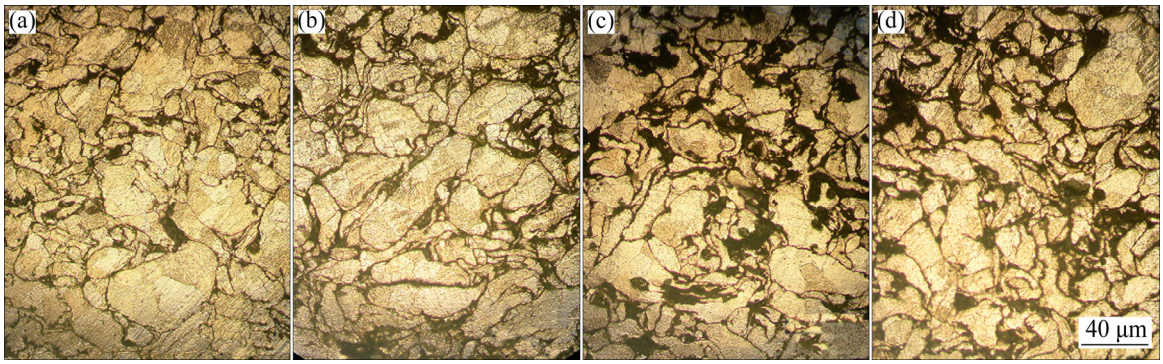

Fig. 2 Optical images of nanocomposites sintered at 550 °C for 2 h: (a) MZC; (b) MZC-1nHA; (c) MZC-2.5nHA; (d) MZC-5nHA

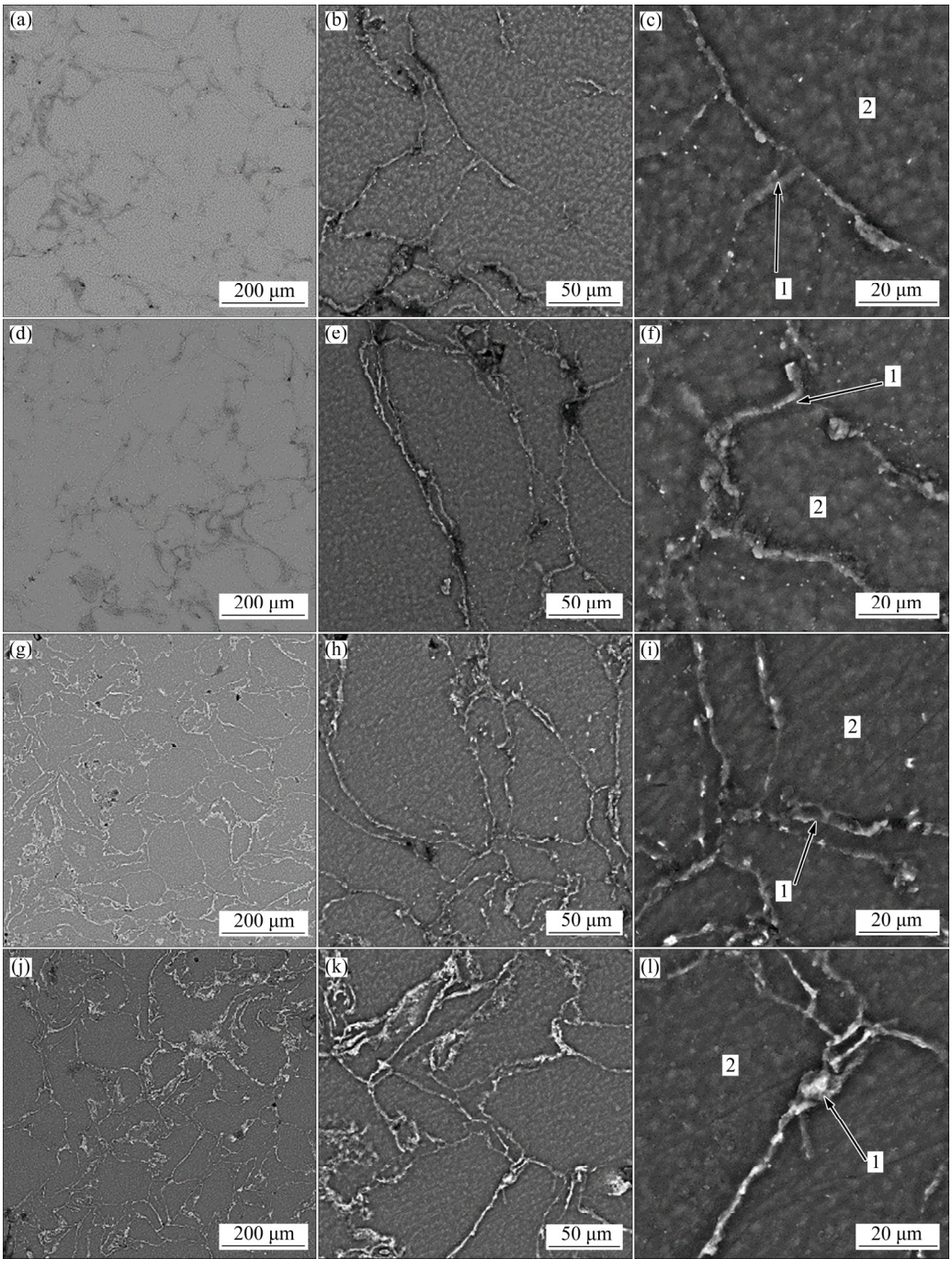

Fig. 3 SEM micrographs of nanocomposites: (a−c) MZC; (d−f) MZC-1nHA; (g−i) MZC-2.5nHA; (j−l) MZC-5nHA

Table 1 Compositions of marked points in Fig. 3 for MZC, MZC-1nHA, MZC-2.5nHA and MZC-5nHA nanocomposites (mass fraction, %)

Sample	Point 1				Point 2			
	Mg	Zn	Ca	P	Mg	Zn	Ca	P
MZC	91.39	8.44	0.14	−	95.53	4.47	−	−
MZC-1nHA	92.77	6.87	0.22	0.14	95.72	4.28	−	−
MZC-2.5nHA	90.17	3.51	3.9	2.42	95.03	4.97	−	−
MZC-5nHA	82.55	7.12	6.32	4.01	95.95	4.05	−	−

3.2 In vitro corrosion measurements

Figure 4 illustrates the electrochemical polarization curves for nanocomposites. As shown, corrosion potential (φ_{corr}) and corrosion current density (J_{corr}) of MZC were improved by adding HA nano particles as reinforcement. The φ_{corr} and J_{corr} values of MZC were changed from −1.72 V and 66 μA/cm^2 to −1.64 V and 30 μA/cm^2, respectively, by compositing with 1% (mass fraction) nHA. The electrochemical parameters of samples acquired from polarization curves are listed in Table 2. Corrosion current densities increased in the order of J_{corr}(MZC-1nHA) < J_{cor}(MZC-2.5nHA) < J_{corr}(MZC) < J_{corr}(MZC-5nHA). In fact, adding nHA into MZC up to 2.5% nHA had a positive effect and caused J_{corr} to decrease but higher than 2.5% nHA caused J_{corr} value to increase.

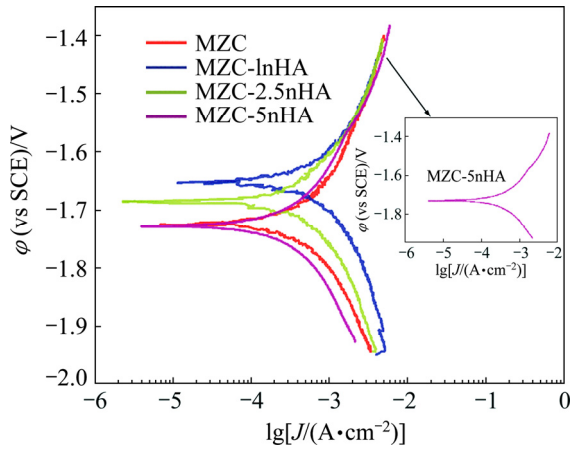

Fig. 4 Electrochemical anodic potentiodynamic polarization curves for samples in SBF solution in ambient conditions

Nyquist, bode and phase angle plots obtained for nanocomposites in SBF are shown in Figs. 5(a−c). The Nyquist plots for MZC alloy consisted of two loops: one capacitance loop in high−medium frequency and the other one, an inductive loop in medium−low frequency. A similar Nyquist plot was reported for Mg−Zn alloy by YAN et al [15]. The Inductive loop in low frequency indicated the inductive behavior for the working electrode [11]. The Nyquist plots for nanocomposites presented two capacitive loops: one in high frequencies related to charge transfer and the other one in low frequencies related to surface protective film effect [28], and one inductive loop was also seen in very low frequency.

Table 2 Electrochemical parameters obtained from Fig. 4

Sample	Anodic slop, β_a/(mv·dec^{-1})	Cathodic slop, $-\beta_c$/(mV·dec^{-1})	Corrosion potential, φ_{corr} (vs SCE)/V	Current density, J_{corr}/(μA·cm^{-2})
MZC	75	74.6	−1.72	66
MZC-1nHA	47.78	56.9	−1.64	30
MZC-2.5nHA	67.9	73.8	−1.68	43
MZC-5nHA	88.4	70.3	−1.72	78

The equivalent circuit acquired from EIS data indicated the corrosion behavior of nanocomposites. The proposed equivalent circuit for nanocomposites is shown in Fig. 5(d). In this model, a constant phase element (CPE) was used instead of capacitive element, which described a non-ideal capacitive behavior [29]. The electrolyte resistance was shown by R_s and high−medium frequency capacitive loop was shown by R_1 and CPE$_1$. R_1 represented the charge transfer resistance associated with the micro-galvanic events, which was paralleled to an electric double layer at the interface of electrolyte solution and magnesium matrix (CPE$_1$). The medium−low frequency capacitive loop was shown by R_2 and CPE$_2$. R_2 and CPE$_2$ indicated the resistance and capacitance of the protective film layer on surface of samples. The inductive element was designated by L.

The fitting results are listed in Table 3. The R_1 of MZC was about 18 Ω·cm^2, whereas it was increased to about 46 Ω·cm^2 for MZC-1nHA. In fact, compositing of MZC with bioactive nanoparticles of nHA motivated the formation of film layer on the surface in SBF solution, which provided an improved protection for MZC matrix.

Corrosion rate of nanocomposites determined by mass loss test is shown in Fig. 6(a). Calculated corrosion rates for all samples were high during the first 24 h of test and after that they decreased slightly until 72 h. The corrosion rate for nanocomposites changed in all immersion times as shown below: MZC-1nHA < MZC-2.5nHA < MZC < MZC-5nHA. This was in good agreement with the polarization test results.

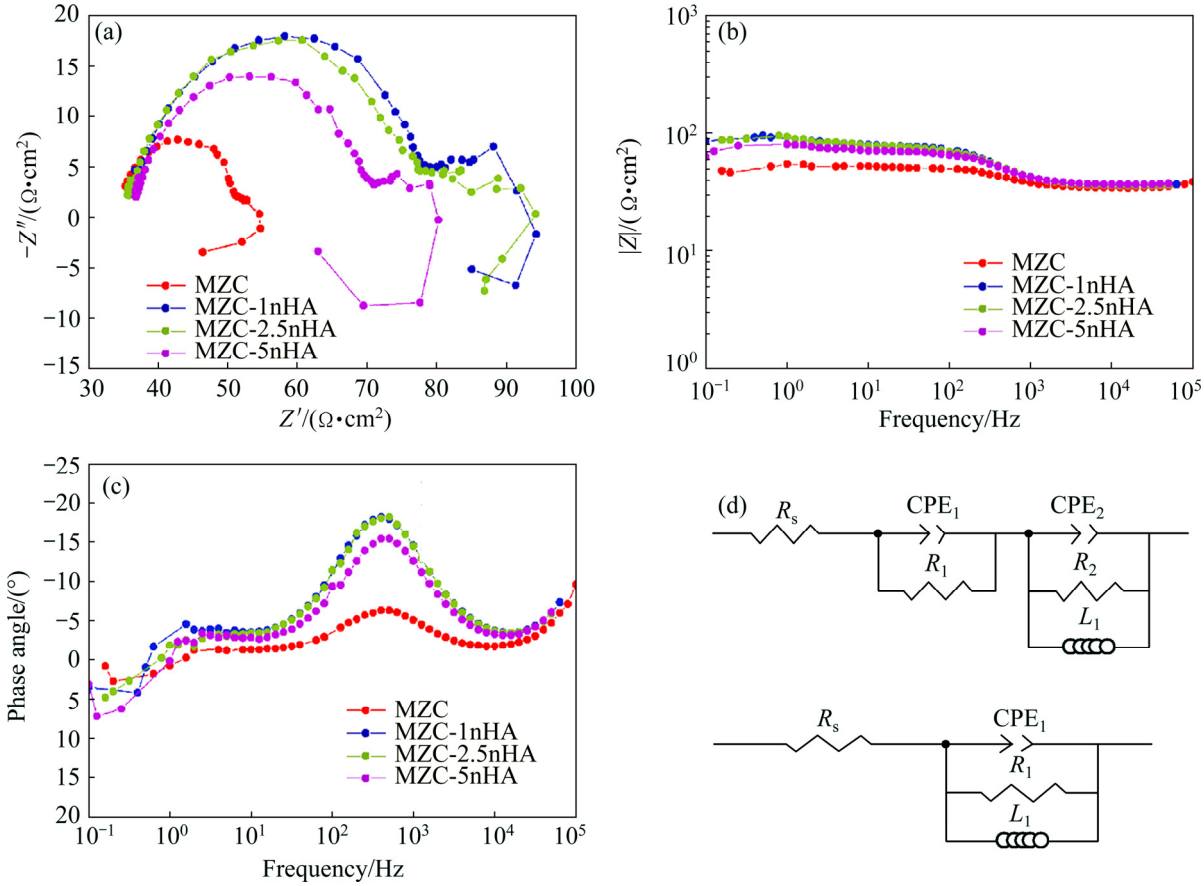

Fig. 5 Nyquist (a), Bode (b), phase angle plots (c), and schematic equivalent circuit (d) for alloy and biocomposite samples in SBF

Table 3 Kinetic parameters obtained from EIS plots for biocomposite samples

Sample	$R_s/(\Omega\cdot cm^2)$	$CPE_1/(\mu F\cdot cm^{-2})$	n_1	$R_1/(\Omega\cdot cm^2)$	$CPE_2/(\mu F\cdot cm^{-2})$	n_2	$R_2/(\Omega\cdot cm^2)$
MZC	36.52	1.28×10^{-5}	0.86	18.4052			
MZC-1nHA	36.52	1.19×10^{-3}	0.86	46.2	6.16×10^{-6}	0.88	42.0816
MZC-2.5nHA	36.52	1.01×10^{-3}	0.87	13.5916	6.16×10^{-6}	0.89	40.3348
MZC-5nHA	36.52	2.33×10^{-3}	0.75	28.6968	7.48×10^{-6}	0.88	33.3828

According to Eq. (3), the degradation rate of magnesium was also monitored by the evolved hydrogen volume and the released Mg ions. In fact, 1 mol of H_2 gas (22.4 L) is directly related to the dissolution of 1 mol of Mg (24.31 g) [23]:

$$Mg+2H_2O=Mg^{2+}+2OH^-+H_2\uparrow \quad (3)$$

Figures 6(b) and (c) present the results of the hydrogen evolution and amount of Mg ion in SBF as a function of immersion time for nanocomposites, respectively. In accordance with mass loss results, the volume of H_2 gas and the amount of released Mg ions were high during the first 24 h of test. This could be related to the formation of precipitated layer on samples after 24 h [30]. When the samples were exposed to the SBF, chemical dissolution on the entire surface led to fast degradation and after precipitation of corrosion product it decreased gradually. Furthermore, the above investigation showed that corrosion resistance of MZC was improved by addition of appropriate content of nHA. The role of nHA in blocking the grain growth of matrix [11] and its bioactivity [9] might influence the corrosion mechanism of Mg alloy.

Different redox potential between Mg (−2.37 V (vs SCE)) [31] and eutectic phases Mg_2Ca (−1.54V (vs SCE)) and $MgZn_2$ (−0.76 V (vs SCE)) created galvanic corrosion on MZC surface in SBF [2]. The galvanic corrosion would accelerate the degradation of Mg alloy and led to a localized corrosion attack on surface. Most of the corrosion products such as $Mg(OH)_2$ are not stable in the presence of chloride ions in SBF solution and transformed into soluble components like $MgCl_2$ and did

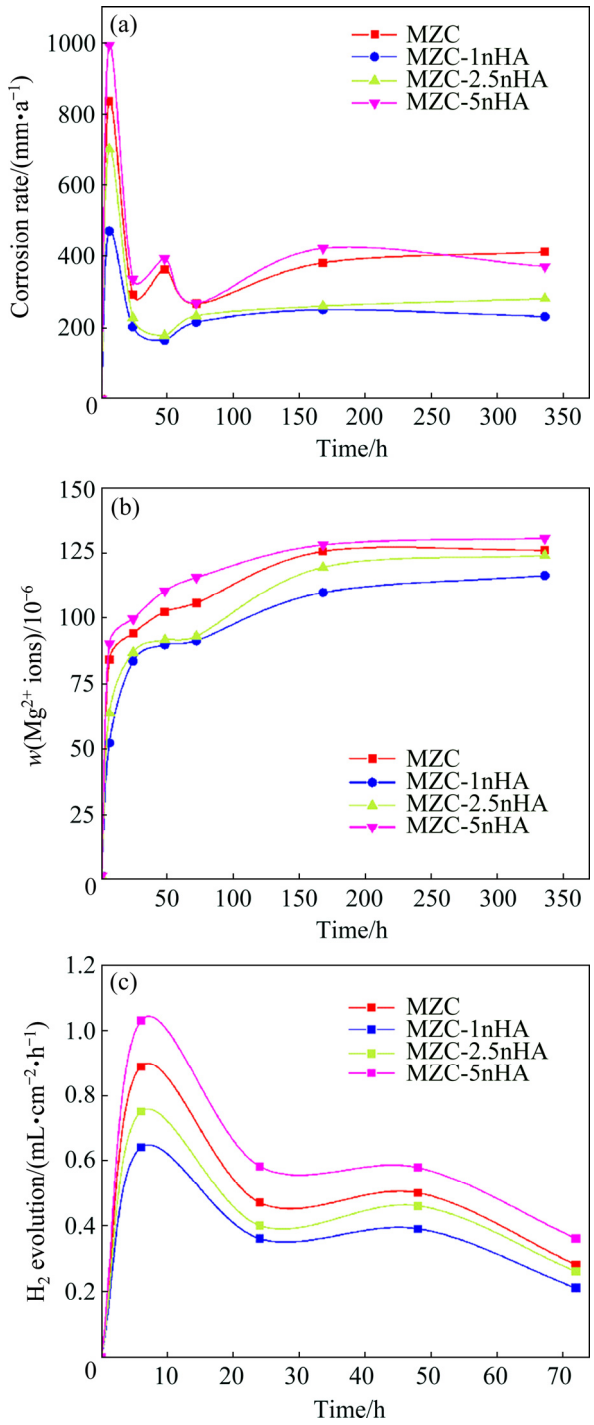

Fig. 6 Variation in corrosion rate (a), content of Mg ion (b) and H_2 evolution (c) for MZC, MZC-1nHA, MZC-2.5nHA and MZC-5nHA after immersing in SBF solution for different time

not avoid the corrosion of MZC. SEM micrograph of MZC immersed in SBF for 72 h are shown in Fig. 7(a) which confirmed the presence of some cracks on the surface and revealed that precipitated layers could not cover all the surface and some parts of alloy were directly in contact with the medium.

Two mechanisms may be suggested for describing the effect of HA particles on corrosion properties of Mg and its alloys: 1) HA particles as reinforcement, motivate the formation of chemically-stable layers on surface [9]. This layer may prevent access of media to the surface and protect the Mg composites. 2) Addition of HA particles into Mg alloy as reinforcement makes its microstructure refined and this fine microstructure increases corrosion resistance of nanocomposites through three approaches: acceleration in formation of oxide film on surface, increasing adhesiveness of oxide film at grain boundaries and a decrease in galvanic couple between grain interior and grain boundaries [11].

In this work, the OM images of samples showed an increase in the amounts of nHA, which restricted the growth of grain in sintering process and decreased the grain size of nanocomposites. The SEM micrographs for nanocomposites immersed in SBF for 72 h is shown in Figs. 7(c−d), indicating a surface covered with a protective precipitated layer. FTIR spectrum for this layer on MZC-1nHA illustrated that phosphate, carbonate and hydroxide components were precipitated on the surface (see Fig. 8). Phosphate and carbonate components like calcium phosphate and calcium carbonate were stable, which might limit the corrosion of nanocomposites. Therefore, the presence of bioactive nHA in Mg structure accelerated the formation of chemically-stable layers on surface, which limited the access of solution at surface and improved the corrosion rate of MZC. Therefore, according to both theories, it is expected that corrosion resistance of nanocomposites could be increased by increasing the contents of nHA. However, the results of electrochemical and emission tests revealed that the nanocomposite with 1% (mass fraction) nHA had the best corrosion resistance among the others. AHMADKHANIHA et al [11] and GU et al [32] investigated the corrosion properties of Mg/HA composite and reported that the presence of interface between HA and Mg breaking the continuity of Mg matrix created preferential locations for corrosion attacks. As a result, increasing the contents of nHA in nanocomposites, from one aspect increased the localized corrosion in interfaces with matrix and from other aspect proliferated the density of precipitated layer. The SEM images of the precipitation layer in Figs. 7(b−d) revealed that an increase in nHA content increased the density of the layer. At the early stage of corrosion, the gas products from localized corrosion (like H_2) were accumulated under the dense precipitated layer and caused the layer to swell and as a result its adhesiveness to surface was reduced. Figure 7(d) shows this swollen layer on MZC-5nHA surface. The anodic branch of polarization curve for MZC-5nHA in Fig. 4 showed a break-down in potential which was an indication of a rupture in

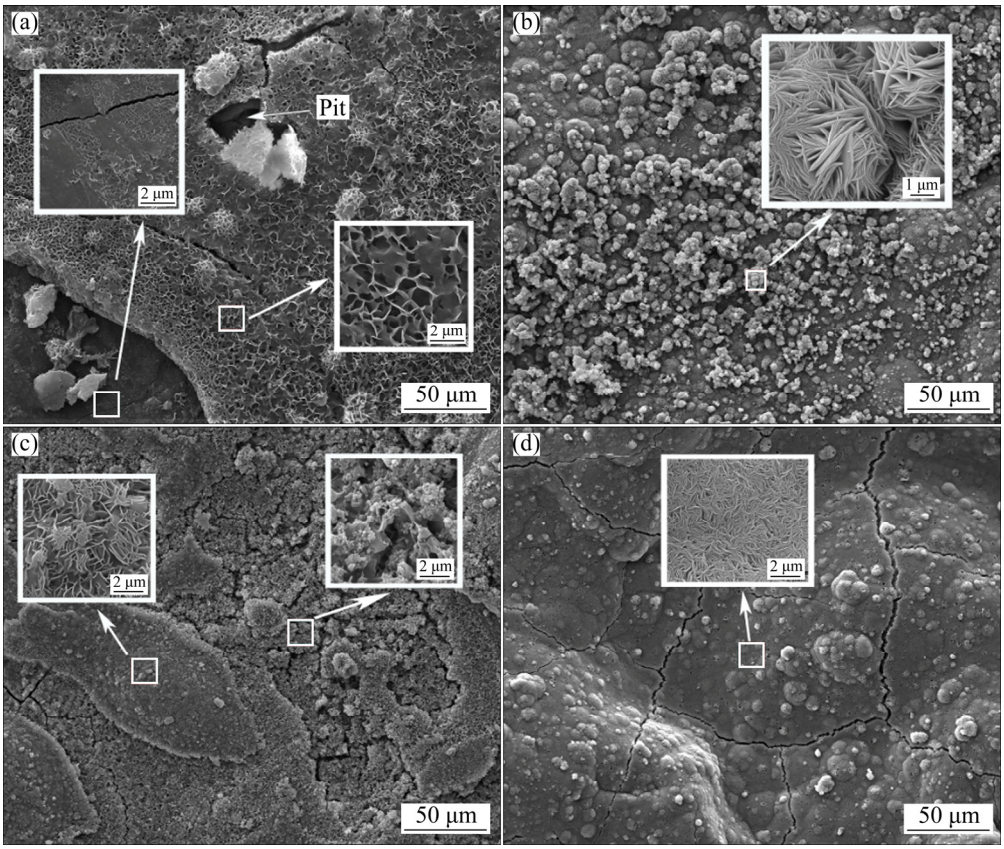

Fig. 7 SEM photomicrographs of MZC (a), MZC-1nHA (b), MZC-2.5nHA (c) and MZC-5nHA (d) after 72 h of immersion in SBF under physiological condition of 5% CO_2 at 37 °C

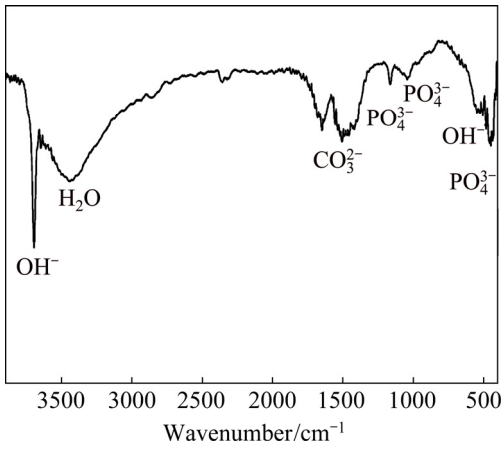

Fig. 8 FTIR spectrum for corrosion product for MZC-1nHA after 72 h of immersion in SBF

precipitated layer. Break-down in the layer allowed the solution to penetrate to the surface and caused the corrosion rate of MZC-5nHA to increase. A fluctuation in calculated corrosion rate for MZC-5nHA in Fig. 6 at 48 h could confirm this mater.

3.3 MTT assay

The RGR of cells in extracted solutions for nanocomposites is shown in Fig. 9. The RGR results for control and specimens revealed that there was no toxicity in three-day extracted solutions. A comparison between the RGR for extracted solution of MZC with that of nanocomposites showed that adding nHA as reinforcement into MZC might increase the RGR of cells. The RGR for 5- and 7-day extractions of MZC showed about 42%−45% reduction in comparison with that of control. This might be due to the pH of extraction

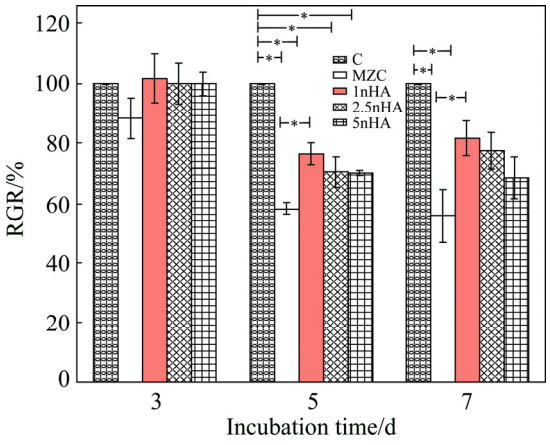

Fig. 9 RGR of MG63 cells in extracted solutions of nanocomposites after incubating in RPMI for 3, 5 and 7 days (*$p < 0.05$)

which was increased as a result of Mg corrosion [33]. The pH values for 7-day extractions of MZC, MZC-1nHA, MZC-2.5nHA and MZC-5nHA nanocomposites were (11.02±0.11), (10.21±0.12), (10.42±0.16) and (10.83±0.13), respectively. High pH was not an appropriate condition for cell to grow [34]. The highest relative growth rate for MG63 cells was acquired in MZC-1nHA extraction solutions which showed the lowest corrosion rate. The RGR of cells decreased with an increase in nHA content of nanocomposites.

4 Conclusions

1) Addition of bioactive nHA to Mg alloy affected the corrosion rate of Mg alloy in SBF by motivating the formation of stable phosphate and carbonate layers on surface.

2) Addition of large contents of nHA in Mg alloy as reinforcements introduced some corroded sites at interface with Mg alloy. In addition, an increase in the density of precipitated layer was observed after immersing in SBF.

3) Gases produced from localized corrosion were accumulated underneath the precipitated layer and decreased its adhesiveness and lowered its corrosion resistance.

4) MTT assay showed that nanocomposite extraction medium did not induce toxicity for MG63 cells and the extraction media for MZC-1nHA showed almost similar behavior as negative control.

References

[1] WITTE F, ULRICH H, RUDERT M, WILLBOLD E. Biodegradable magnesium scaffolds. Part 1: Appropriate inflammatory response [J]. Journal of Biomedical Materials Research Part A, 2007, 81(3): 748−756.

[2] YIN Ping, LI Nian-feng, LEI Ting, LIU Lin, OUYANG Chun. Effects of Ca on microstructure, mechanical and corrosion properties and biocompatibility of Mg−Zn−Ca alloys [J]. Journal of Materials Science: Materials in Medicine, 2013, 24(6): 1365−1373.

[3] ALVAREZ-LOPEZ M, PEREDA M D, DEL VALLE J A, FERNANDEZ-LORENZO M, GARCIA-ALONSO M C, RUANO O A, ESCUDERO M L. Corrosion behaviour of AZ31 magnesium alloy with different grain sizes in simulated biological fluids [J]. Acta Biomaterialia, 2010, 6(5): 1763−1771.

[4] DU Hui, WEI Zun-jie, LIU Xin-wang, ZHANG Er-lin. Effects of Zn on the microstructure, mechanical property and bio-corrosion property of Mg−3Ca alloys for biomedical application [J]. Materials Chemistry and Physics, 2011, 125(3): 568−575.

[5] GU Xue-nan, ZHENG Yu-feng. A review on magnesium alloys as biodegradable materials [J]. Frontiers of Materials Science in China, 2010, 4(2): 111−115.

[6] STAIGER M P, PIETAK A M, HUADMAIUADMAI J, DIAS G. Magnesium and its alloys as orthopedic biomaterials: A review [J]. Biomaterials, 2006, 27(9): 1728−1734.

[7] ZHANG Shao-xiang, ZHANG Xiao-nong, ZHAO Chang-li, LI Jia-nan, SONG Yang, XIE Chao-ying, TAO Hai-rong, ZHANG Yan, HE Yao-hua, JIANG Yao, BIAN Yu-jun. Research on an Mg−Zn alloy as a degradable biomaterial [J]. Acta biomaterialia, 2010, 6(2): 626−640.

[8] ZHENG Y F, GU X N, XI Y L, CHAI D L. In vitro degradation and cytotoxicity of Mg/Ca composites produced by powder metallurgy [J]. Acta Biomaterialia, 2010, 6(5): 1783−1791.

[9] RAZAVI M, FATHI M H, MERATIAN M. Fabrication and characterization of magnesium–fluorapatite nanocomposite for biomedical applications [J]. Materials Characterization, 2010, 61(12): 1363−1370.

[10] FENG Ai-ling, HAN Yong. Mechanical and in vitro degradation behavior of ultrafine calcium polyphosphate reinforced magnesium-alloy composites [J]. Materials & Design, 2011, 32(5): 2813−2820.

[11] AHMADKHANIHA D, FEDEL M, SOHI M H, HANZAKI A Z, DEFLORIAN F. Corrosion behavior of magnesium and magnesium–hydroxyapatite composite fabricated by friction stir processing in Dulbecco's phosphate buffered saline [J]. Corrosion Science, 2016, 104: 319−329.

[12] YANG Hua-wei, XIA Ka-da, WANG Tao-lei, NIU Jun-chao, SONG Yi-ming, XIONG Zu-quan, ZHENG Kui, WEI Shi-qing, LU Wei. Growth, in vitro biodegradation and cytocompatibility properties of nano-hydroxyapatite coatings on biodegradable magnesium alloys [J]. Journal of Alloys and Compounds, 2016, 672: 366−373.

[13] SHADANBAZ S, DIAS G J. Calcium phosphate coatings on magnesium alloys for biomedical applications: A review [J]. Acta Biomaterialia, 2012, 8(1): 20−30.

[14] WANG H X, GUAN S K, WANG X, REN C X, WANG L G. In vitro degradation and mechanical integrity of Mg−Zn−Ca alloy coated with Ca-deficient hydroxyapatite by the pulse electrodeposition process [J]. Acta Biomaterialia, 2010, 6(5): 1743−1748.

[15] YAN Yang, KANG Yi-jun, LI Ding, YU Kun, XIAO Tao, DENG You-wen, DAI Han, DAI Yi-long, XIONG Han-qing, FANG Hong-jie. Improvement of the mechanical properties and corrosion resistance of biodegradable β-$Ca_3(PO_4)_2$/Mg−Zn composites prepared by powder metallurgy: The adding β-$Ca_3(PO_4)_2$, hot extrusion and aging treatment [J]. Materials Science and Engineering C, 2017, 74: 582−596.

[16] ZHANG Bao-ping, WANG Yin, GENG Lin. Research on Mg−Zn−Ca alloy as degradable biomaterial [M]. Biomaterials−Physics and Chemistry, 2011: 184−204.

[17] TONG L B, ZHENG Ming-yi, XU Shi-wei, KAMADO S, DU Yu-zhou, HU Xiao-shi, WU K, GAN Wei-min, BROKMEIER H G, WANG G J, LV X Y. Effect of Mn addition on microstructure, texture and mechanical properties of Mg−Zn−Ca alloy [J]. Materials Science and Engineering A, 2011, 528(10): 3741−3747.

[18] HOMMA T, MENDIS C, HONO K, KAMADO S. Effect of Zr addition on the mechanical properties of as-extruded Mg−Zn−Ca−Zr alloys [J]. Materials Science and Engineering A, 2010, 527(9): 2356−2362.

[19] ABOUDZADEH N, IMANI M, SHOKRGOZAR M A, KHAVANDI A, JAVADPOUR J, SHAFIEYAN Y, FAROKHI M. Fabrication and characterization of poly(D,L-lactide-co-glycolide)/hydroxyapatite nanocomposite scaffolds for bone tissue regeneration [J]. Journal of Biomedical Materials Research Part A, 2010, 94(1): 137−145.

[20] KOKUBO T, TAKADAMA H. How useful is SBF in predicting in vivo bone bioactivity? [J] Biomaterials, 2006, 27(15): 2907−2915.

[21] ASTM G31−72. Standard practice for laboratory immersion corrosion testing of metals [S]. Philadelphia, PA, USA: ASTM International, 2004.

[22] ASTM G1−03−E. Standard practice for preparing, cleaning, and evaluating corrosion test specimens [S]. Philadelphia, PA, USA: ASTM International, 2011.

[23] KIRLAND N T, BIRBILIS N, STAIGER M P. Assessing the

corrosion of biodegradable magnesium implants: A critical review of current methodologies and their limitations [J]. Acta Biomaterialia, 2012, 8: 925−936.

[24] XIN Yun-chang, LIU Cheng-long, ZHANG Xin-meng, TANG Guo-yi, TIAN Xiu-bo, CHU P K. Corrosion behavior of biomedical AZ91 magnesium alloy in simulated body fluids [J]. Journal of Material Research, 2007, 22(7): 2004−2011.

[25] ISO-10993-5. Biological evaluation of medical devices–Part 5: Tests for cytotoxicity: In vitro methods [S]. ANSI/AAMI: Arlington, 1999, 10993−10995.

[26] TONG L B, ZHENG M Y, CHANG H, HU X S, WU K, XU S W, KAMADO S, KOJIMA Y. Microstructure and mechanical properties of Mg−Zn−Ca alloy processed by equal channel angular pressing [J]. Materials Science and Engineering A, 2009, 523(1): 289−294.

[27] KHALIL K A. A new-developed nanostructured Mg/HAp nanocomposite by high frequency induction heat sintering process [J]. International Journal of Electrochemical Science, 2012, 7(11): 10698−10710.

[28] KHALAJABADI S Z, KADIR M R A, IZMAN S, MARVIBAIGI M. The effect of MgO on the biodegradation, physical properties and biocompatibility of a Mg/HA/MgO nanocomposite manufactured by powder metallurgy method [J]. Journal of Alloys and Compounds, 2016, 655: 266−280.

[29] LASIA A. Electrochemical impedance spectroscopy and its applications. Modern aspects of electrochemistry [M]. Springer, 2002.

[30] KIM Woo-Cheol, KIM Jung-Gu, LEE Ji-Young, SEOK Hyun-Kwang. Influence of Ca on the corrosion properties of magnesium for biomaterials [J]. Materials Letters, 2008, 62(25): 4146−4148.

[31] YU Kun, CHEN Liang-jian, ZHAO Jun, LI Shao-jun, DAI Yi-long, HUANG Qiao, YU Zhi-ming. In vitro corrosion behavior and in vivo biodegradation of biomedical b-$Ca_3(PO_4)_2$/Mg−Zn composites [J]. Acta Biomaterialia, 2012, 8: 2845−2855.

[32] GU Xue-nan, ZHOU Wei-rui, ZHENG Yu-feng, DONG Li-min, XI Yu-lin, CHAI Dong-lang. Microstructure, mechanical property, bio-corrosion and cytotoxicity evaluations of Mg/HA composites [J]. Materials Science and Engineering C, 2010, 30(6): 827−832.

[33] XIONG Guang-yao, NIE Yan-jiao, JI De-hui, LI Jing, LI Chun-zhi, LI Wei, ZHU Yong, LUO Hong-lin, WAN Yi-zao. Characterization of biomedical hydroxyapatite/ magnesium composites prepared by powder metallurgy assisted with microwave sintering [J]. Current Applied Physics, 2016, 16(8): 830−836.

[34] GU Xue-nan, ZHENG Yu-feng, CHENG Yan, ZHONG Sheng-ping, XI Ting-fei. In vitro corrosion and biocompatibility of binary magnesium alloys [J]. Biomaterials, 2009, 30(4): 484−498.

粉末冶金法制备的 Mg−5Zn−0.3Ca/nHA 生物复合材料的体外降解和细胞毒性

Neda ABOUDZADEH[1], Changiz DEHGHANIAN[1], Mohammad Ali SHOKRGOZAR[2]

1. School of Metallurgy and Materials Engineering, College of Engineering, University of Tehran, P. O. Box 14155-6455, Tehran, Iran;
2. National Cell Bank, Pasteur Institute of Iran, P. O. Box 1316943551, Tehran, Iran

摘　要：采用纯 Mg、Zn、Ca 粉末和纳米羟基磷灰石(nHA) 粉末，通过粉末冶金方法制备 Mg−5Zn−0.3Ca/nHA 生物复合材料，研究不同 nHA 增强相含量 (1%、2.5%和 5%，质量分数) 对 Mg−5Zn−0.3Ca 合金腐蚀性能的影响。通过模拟体液浸泡试验和电化学技术测试其耐腐蚀性。结果显示，添加 1%和 2.5% 的 nHA 提高镁合金的耐腐蚀性，这是因为生物活性 nHA 促进稳定的磷酸盐和碳酸盐表面沉积层的形成，从而提高纳米复合材料的耐蚀性。然而，在镁合金中添加更高含量的 nHA 作为增强相时，表面沉积层的密度增加，导致局部腐蚀产生的气体无法及时排出而聚集在沉积层下，减小层与基体的粘着力，导致耐腐蚀性能下降。对镁合金及其纳米复合材料的间接细胞毒性评价表明其浸提液无细胞毒性，添加 1% nHA 的纳米复合材料的测试结果与阴性对照组几乎相似。

关键词：粉末冶金；金属生物复合材料；腐蚀；镁

(Edited by Bing YANG)